Electronic Research Archive

https://www.aimspress.com/journal/era

ERA, 33(9): 5748–5768.
DOI: 10.3934/era.2025255
Received: 04 August 2025
Revised: 13 September 2025
Accepted: 18 September 2025
Published: 25 September 2025

Research article

Stability analysis for the maximum principle preserving finite difference approach of the surface Allen–Cahn equation on curved surfaces

Hyundong Kim[1,2], Jian Wang[3], Seokjun Ham[4], Youngjin Hwang[4], Jyoti[5] and Junseok Kim[4,*]

[1] Department of Mathematics and Physics, Gangneung-Wonju National University, Gangneung 25457, Republic of Korea

[2] Institute for Smart Infrastructure, Gangneung-Wonju National University, Gangneung 25457, Republic of Korea

[3] School of Mathematics and Statistics, Nanjing University of Information Science and Technology, Nanjing 210044, China

[4] Department of Mathematics, Korea University, Seoul 02841, Republic of Korea

[5] The Institute of Basic Science, Korea University, Seoul 02841, Republic of Korea

* **Correspondence:** Email: cfdkim@korea.ac.kr.

Abstract: A stability analysis of a finite difference scheme was presented for the surface Allen–Cahn (AC) equation on curved surfaces. The surface was discretized by a triangular mesh, which accurately represented geometric features and enabled subsequent computational analysis. A discrete Laplace–Beltrami operator was used on this mesh, and it produced a simple and efficient discrete equation. The explicit time-stepping method, although straightforward, requires a moderate restriction on the time step. For practical applications, it is essential to determine the maximum value of this restriction. We derived the theoretical maximum value of the admissible time step that guarantees the discrete maximum principle and analyzed the stability of the explicit scheme under this condition. Numerical tests were performed to verify the theoretical prediction. The computational results confirmed that the proposed scheme maintains stability and reproduces expected interfacial dynamics on curved geometries. The analysis provides rigorous guidance for selecting stable time steps and demonstrates that the fully explicit scheme can be used as a reliable tool for simulating curvature-driven phase transitions and interfacial motion. This work provides a solid theoretical foundation for explicit numerical methods applied to the surface AC equation and contributes to the improvement of both efficiency and accuracy in computational studies involving complex geometries.

Keywords: stability analysis; Laplace–Beltrami operator; maximum principle preserving

1. Introduction

The Allen–Cahn (AC) equation [1] models the time evolution of an order parameter. The surface AC equation extends this equation to manifolds and thus accounts for the effects of surface curvature. The surface AC equation models the motion of interfaces, such as those arising in two-phase transitions in alloys [2]. The AC-type equations are phase-field models widely used to describe interfacial dynamics under curvature effects. Their applications span multiple disciplines: in materials science, they model alloy phase transitions and dendritic growth on curved surfaces [3, 4]; in biology, they explain curvature-driven phase separation in lipid bilayers and membranes [5–7]; and in imaging, modified AC formulations are applied to reconstruction, denoising, and segmentation tasks [8–12]. They have also been applied to shape transformation and pattern formation [13–19]. These broad applications establish the AC equation as a unifying framework for curvature-dependent interfacial motion. Recent advances in computations on complex surfaces, such as [20–26], have introduced improved discretizations and stability strategies for partial differential equations (PDEs) on nontrivial geometries. Distinct from these contributions, our work provides a rigorous stability analysis of a fully explicit finite difference scheme for the surface AC equation and derives a sharp theoretical bound for the maximum time step that guarantees the discrete maximum principle [27].

Mean curvature flow is a fundamental geometric concept describing the evolution of an interface driven by its mean curvature [28–31]. This process is related to how an interface changes shape as it moves in the direction of its mean curvature at each point. Motion by mean curvature of the AC equation on surfaces has been studied [32]. To numerically implement curvature-driven motion of the AC equation on surfaces, several approaches have been proposed, including operator splitting and closest point methods in narrow band domains. To model general motion by mean curvature, the authors in [33] proposed the modified AC equation with a growth or decay source term. Recently, the authors in [34] investigated motion by mean curvature up to the singularity using the AC equation with a temporally varying interface width parameter.

As in the related works mentioned above, we apply the concept of motion by mean curvature and validate computational simulations on surfaces for the stability analysis of the explicit temporal method. The applied fully explicit temporal method consists of a straightforward discretization of the Laplace–Beltrami operator [35] and the explicit Euler method [13, 36]. The authors solved the AC and conservative AC models on surfaces using the Laplace–Beltrami operator in [2]. The authors in [37] performed stability analysis of the surface AC equation by using first- and second-order stabilized semi-implicit methods, which were based on the surface finite element method. In addition, the authors compared their results with the solution obtained by the operator splitting method and stated that first-order methods are better in stability and can guarantee energy decay, but lack accuracy, whereas a second-order stabilized semi-implicit method is more accurate but requires a smaller time step size to achieve energy stability. Moreover, the second-order operator splitting method may not be suitable for solving the surface AC equation. Previously, there was no theoretical determination of the exact maximum time step size for an explicit method for the surface AC model, hence one had to use an arbitrarily small time step size. The main purpose of this article is to determine, through theoretical analysis, the maximum time step size that guarantees the discrete maximum principle for the fully explicit surface AC scheme.

However, Xiao et al. later modified their scheme [38], originally proposed in [37], by introducing

the lumped mass forms to solve the standard surface AC equation while preserving the discrete maximum principle [27]. Furthermore, Mohammadi et al. [39] studied the convergence of the AC equation on surfaces under no-boundary conditions using a kernel collocation method combined with an explicit time-splitting algorithm. They found that the method was stable under specific conditions, but they could not determine the maximum admissible time step.

The AC equation on surfaces has been extensively studied using semi-implicit and stabilized schemes [37, 38, 40], as they alleviate the severe time step restriction of explicit methods. However, in practice, explicit schemes remain attractive due to their simplicity, ease of implementation, and natural parallelism. Despite these advantages, the fully explicit surface AC scheme has been less analyzed because of the stringent Courant–Friedrichs–Lewy (CFL)-type condition [41], and most prior studies have used only arbitrarily small time steps without theoretical justification. A rigorous stability analysis of the fully explicit method is therefore essential to establish when such schemes can be used reliably. In particular, determining the sharp maximum admissible time step that guarantees the discrete maximum principle provides both theoretical understanding and practical guidance. This study is motivated by the need to close this gap: we focus on the stability of the fully explicit finite difference scheme for the surface AC equation and derive an explicit bound for the time step that ensures stability and consistency with the maximum principle.

The outline of this study is as follows. In Section 2, we consider a surface AC model and its numerical scheme. In Section 3, we perform a stability analysis of the proposed explicit time-stepping approach. In Section 4, the computational tests are conducted. Conclusions are given in Section 5.

2. Computational method

On a smooth closed surface $\mathcal{S}$, we shall analyze the surface AC equation:

$$\frac{\partial \phi(\mathbf{x},t)}{\partial t} = -\frac{F'(\phi(\mathbf{x},t))}{\epsilon^2} + \Delta_{\mathcal{S}}\phi(\mathbf{x},t), \tag{2.1}$$

where ϕ is the order parameter, $\epsilon > 0$, $F(\phi(\mathbf{x},t)) = (\phi^2(\mathbf{x},t)-1)^2/4$, and $\Delta_{\mathcal{S}}$ is the Laplace–Beltrami operator. Note that Eq (2.1) is posed on a closed smooth surface without boundary; therefore, no boundary conditions are required. To solve the surface AC equation, the discretization of the Laplace–Beltrami operator is considered. The computational setting for our study is schematically illustrated in Figure 1(a–d), where the triangulated surface M, one-ring neighbors, and local areas are displayed. This provides a clear depiction of the geometric discretization used in our analysis. Let $\{\mathbf{x}\}_{i=1}^{N}$ be the surface vertex set. Figure 1(b) displays $V(i) = \{i_1, i_2, \cdots, i_m\}$ of the one-ring neighbor vertex indices at $\mathbf{x}_i$, see [42] for definitions of the additional notations and more details.

The area of triangle T_j in contact with $\mathbf{x}_i$ is denoted by $A(\mathbf{x}_i, T_j)$ and is defined as follows:

$$\begin{aligned} A(\mathbf{x}_i, T_j) &= \frac{1}{2}|\mathbf{x}_j - \mathbf{x}_i||\mathbf{x}_{j_-} - \mathbf{x}_i| \sin\theta = \frac{1}{2}|\mathbf{x}_j - \mathbf{x}_i||\mathbf{x}_{j_-} - \mathbf{x}_i| \sqrt{1-\cos^2\theta} \\ &= \frac{1}{2}\sqrt{|\mathbf{x}_j - \mathbf{x}_i|^2|\mathbf{x}_{j_-} - \mathbf{x}_i|^2 - |\mathbf{x}_j - \mathbf{x}_i|^2|\mathbf{x}_{j_-} - \mathbf{x}_i|^2\cos^2\theta} \\ &= \frac{1}{2}\sqrt{|\mathbf{x}_j - \mathbf{x}_i|^2|\mathbf{x}_{j_-} - \mathbf{x}_i|^2 - \left(\mathbf{x}_j - \mathbf{x}_i, \mathbf{x}_{j_-} - \mathbf{x}_i\right)^2}. \end{aligned} \tag{2.2}$$

Therefore, we define $A(\mathbf{x}_i) = \sum_{j\in V(i)} A(\mathbf{x}_i, T_j)$. Let us denote $\phi_i = \phi(\mathbf{x}_i)$. Then, the Laplace–Beltrami operator can be discretized as follows:

$$\Delta_S \phi_i = \frac{3}{A(\mathbf{x}_i)} \sum_{j\in V(i)} \frac{\cot\theta_{ij} + \cot\theta_{ij_+}}{2}(\phi_j - \phi_i), \tag{2.3}$$

where θ_{ij} is the angle in triangle T_j [43,44]. In this study, the Laplace-Beltrami operator is discretized using the cotangent formula on triangulated surfaces. The construction is applicable to general triangular meshes under the standard shape-regularity assumption, i.e., the mesh elements are non-degenerate with interior angles bounded away from zero and element areas bounded away from vanishing values. Such a minimum angle condition is sufficient to guarantee that the cotangent weights are well defined and that the discrete Laplace-Beltrami operator converges to the continuous Laplace–Beltrami operator [35,43,44]. The fully explicit Euler method is applied to solve the AC equation (2.1) computationally. The fully explicit scheme, despite its restriction on the time step size, is simple and easy to implement. In contrast, implicit schemes theoretically allow larger time steps, but in practice the step size is often limited by accuracy considerations. For second-order PDEs such as the AC equation, implicit methods may be efficient, while for fourth-order PDEs such as the Cahn–Hilliard (CH) equation, the computational cost of solving the implicit system becomes significantly higher. Therefore, in this work we adopt the explicit scheme to balance between clarity, simplicity, and computational feasibility.

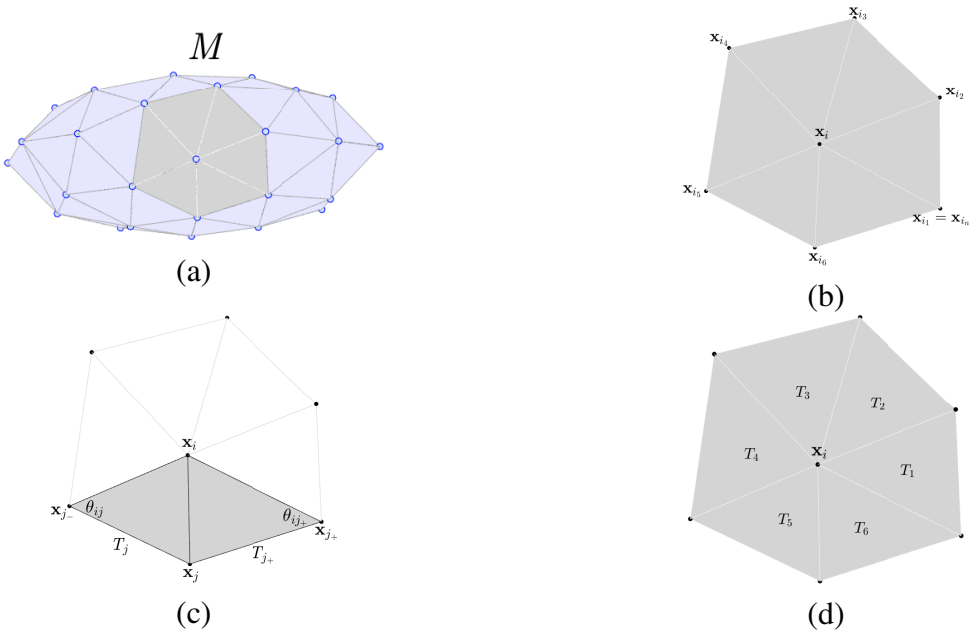

Figure 1. Schematic illustrations of (a) the triangulated surface, (b) one-ring neighbors of $\mathbf{x}_i$ with $i_1 = i_n$, (c) triangles T_j and T_{j+}, and (d) area $A(\mathbf{x}_i)$ on triangular surface M.

Remark. The computational cost of the explicit finite difference scheme is relatively low per time step, since only local stencil operations are required on the triangulated surface without solving global linear systems. However, the scheme is subject to a CFL-type restriction, which limits the admissible time

step size and may increase the number of iterations in long-time simulations. Despite this limitation, the locality of the scheme allows for straightforward parallelization and efficient scalability on modern computational platforms such as multi-core CPUs and GPUs.

For $i = 1, \ldots, N$,

$$\frac{\phi_i^{n+1} - \phi_i^n}{\Delta t} = \frac{\phi_i^n - (\phi_i^n)^3}{\epsilon^2} + \Delta_S \phi_i^n, \tag{2.4}$$

which can be rewritten as follows:

$$\phi_i^{n+1} = \phi_i^n + \Delta t \left(\frac{\phi_i^n - (\phi_i^n)^3}{\epsilon^2} + \Delta_S \phi_i^n \right). \tag{2.5}$$

Note that the accuracy of the discrete Laplace–Beltrami operator depends on the quality and resolution of the triangulated mesh, as finer and more regular elements better capture surface curvature [45]. In addition, the maximum time step restriction is essential for preserving stability and the discrete maximum principle. This bound not only prevents numerical instabilities but also provides a guideline for selecting the largest stable step size and thus improves the efficiency of explicit computations.

3. Stability analysis

We now perform the stability analysis of the fully explicit scheme for the surface AC equation. The maximum norm is defined as follows:

$$\|\phi^n\|_\infty = \max_{1 \le i \le N} |\phi_i^n|.$$

Theorem 1. *Suppose that the initial condition satisfies* $\|\phi^0\|_\infty \le 1$. *Then, the fully explicit approach preserves the boundedness of the computational solutions for all times, i.e., for* $n \ge 0$,

$$\|\phi^{n+1}\|_\infty \le 1, \tag{3.1}$$

if the size of the temporal step satisfies

$$\Delta t \le \min_{1 \le i \le N} \frac{2\epsilon^2 A(\mathbf{x}_i)}{4A(\mathbf{x}_i) + 3\epsilon^2 \sum_{j \in V(i)} \left(\cot \theta_{ij} + \cot \theta_{ij+} \right)}. \tag{3.2}$$

Proof. Equation (2.5) can be rewritten as follows:

$$\phi_i^{n+1} = \phi_i^n + \frac{\Delta t}{\epsilon^2} \left[\phi_i^n - (\phi_i^n)^3 \right] + \frac{3\Delta t}{A(\mathbf{x}_i)} \sum_{j \in V(i)} \frac{\cot \theta_{ij} + \cot \theta_{ij+}}{2} (\phi_j^n - \phi_i^n). \tag{3.3}$$

Case 1. $\phi_i^n = 0$

We can obtain the following inequality from Eq (3.3):

$$|\phi_i^{n+1}| = \left| \frac{3\Delta t}{A(\mathbf{x}_i)} \sum_{j\in V(i)} \frac{\cot\theta_{ij} + \cot\theta_{ij+}}{2} \phi_j^n \right| \le \frac{3\Delta t}{A(\mathbf{x}_i)} \sum_{j\in V(i)} \frac{\cot\theta_{ij} + \cot\theta_{ij+}}{2} \|\phi^n\|_\infty.$$

Therefore, if

$$\Delta t \le \frac{2A(\mathbf{x}_i)}{3\sum_{j\in V(i)} \left(\cot\theta_{ij} + \cot\theta_{ij+}\right)},$$

then $|\phi_i^{n+1}| \le 1$.

Case 2. $\phi_i^n = 1$

$$\begin{aligned}
|\phi_i^{n+1}| &= \left| 1 + \frac{3\Delta t}{A(\mathbf{x}_i)} \sum_{j\in V(i)} \frac{\cot\theta_{ij} + \cot\theta_{ij+}}{2} (\phi_j^n - 1) \right| \\
&= \left| 1 - \frac{3\Delta t}{A(\mathbf{x}_i)} \sum_{j\in V(i)} \frac{\cot\theta_{ij} + \cot\theta_{ij+}}{2} + \frac{3\Delta t}{A(\mathbf{x}_i)} \sum_{j\in V(i)} \frac{\cot\theta_{ij} + \cot\theta_{ij+}}{2} \phi_j^n \right| \\
&\le \left| 1 - \frac{3\Delta t}{A(\mathbf{x}_i)} \sum_{j\in V(i)} \frac{\cot\theta_{ij} + \cot\theta_{ij+}}{2} \right| + \frac{3\Delta t}{A(\mathbf{x}_i)} \sum_{j\in V(i)} \frac{\cot\theta_{ij} + \cot\theta_{ij+}}{2} \|\phi^n\|_\infty. \qquad (3.4)
\end{aligned}$$

If

$$\Delta t \le \frac{2A(\mathbf{x}_i)}{3\sum_{j\in V(i)} \left(\cot\theta_{ij} + \cot\theta_{ij+}\right)},$$

then Eq (3.4) becomes

$$|\phi_i^{n+1}| \le 1 - \frac{3\Delta t}{A(\mathbf{x}_i)} \sum_{j\in V(i)} \frac{\cot\theta_{ij} + \cot\theta_{ij+}}{2} + \frac{3\Delta t}{A(\mathbf{x}_i)} \sum_{j\in V(i)} \frac{\cot\theta_{ij} + \cot\theta_{ij+}}{2} \|\phi^n\|_\infty \le 1.$$

Therefore, we have $|\phi_i^{n+1}| \le 1$.

Case 3. $0 < \phi_i^n < 1$

$$\begin{aligned}
&\phi_i^n + \frac{\Delta t}{\epsilon^2} \left[\phi_i^n - (\phi_i^n)^3 \right] + \frac{3\Delta t}{A(\mathbf{x}_i)} \sum_{j\in V(i)} \frac{\cot\theta_{ij} + \cot\theta_{ij+}}{2} (-1 - \phi_i^n) \le \phi_i^{n+1} \\
&\qquad \le \phi_i^n + \frac{\Delta t}{\epsilon^2} \left[\phi_i^n - (\phi_i^n)^3 \right] + \frac{3\Delta t}{A(\mathbf{x}_i)} \sum_{j\in V(i)} \frac{\cot\theta_{ij} + \cot\theta_{ij+}}{2} (1 - \phi_i^n). \qquad (3.5)
\end{aligned}$$

First, we consider the left-hand side of the inequality (3.5):

$$-1 \le \phi_i^n + \Delta t \left[\frac{\phi_i^n (1 - \phi_i^n)(1 + \phi_i^n)}{\epsilon^2} - \frac{3}{A(\mathbf{x}_i)} \sum_{j\in V(i)} \frac{\cot\theta_{ij} + \cot\theta_{ij+}}{2} (1 + \phi_i^n) \right].$$

The above inequality can be rewritten as

$$-1-\phi_i^n \le \Delta t(1+\phi_i^n)\left[\frac{\phi_i^n(1-\phi_i^n)}{\epsilon^2}-\frac{3}{A(\mathbf{x}_i)}\sum_{j\in V(i)}\frac{\cot\theta_{ij}+\cot\theta_{ij+}}{2}\right].$$

Then, by dividing both sides of the above inequality by $(1+\phi_i^n) > 0$, we can obtain

$$-1 \le \Delta t\frac{\phi_i^n(1-\phi_i^n)\,2A(\mathbf{x}_i)-3\epsilon^2\sum_{j\in V(i)}\left(\cot\theta_{ij}+\cot\theta_{ij+}\right)}{2\epsilon^2A(\mathbf{x}_i)}. \tag{3.6}$$

If the right-hand side in Eq (3.6) is non-negative, then there is no restriction on the time step. Otherwise, if the term is negative, then

$$\Delta t \le \frac{2\epsilon^2A(\mathbf{x}_i)}{3\epsilon^2\sum_{j\in V(i)}\left(\cot\theta_{ij}+\cot\theta_{ij+}\right)-\phi_i^n(1-\phi_i^n)\,2A(\mathbf{x}_i)}.$$

Since $\phi_i^n(1-\phi_i^n) > 0$ holds, we have the following constraint:

$$\Delta t \le \frac{2A(\mathbf{x}_i)}{3\sum_{j\in V(i)}\left(\cot\theta_{ij}+\cot\theta_{ij+}\right)}.$$

Next, we consider the right-hand side of inequality (3.5):

$$\phi_i^n+\Delta t\left[\frac{\phi_i^n(1-\phi_i^n)(1+\phi_i^n)}{\epsilon^2}+\frac{3}{A(\mathbf{x}_i)}\sum_{j\in V(i)}\frac{\cot\theta_{ij}+\cot\theta_{ij+}}{2}(1-\phi_i^n)\right]\le 1.$$

The above inequality can be rewritten as

$$\Delta t(1-\phi_i^n)\left[\frac{\phi_i^n(1+\phi_i^n)}{\epsilon^2}+\frac{3}{A(\mathbf{x}_i)}\sum_{j\in V(i)}\frac{\cot\theta_{ij}+\cot\theta_{ij+}}{2}\right]\le 1-\phi_i^n.$$

By dividing both sides of the above inequality by $(1-\phi_i^n) > 0$, we get

$$\Delta t\left(\frac{2\phi_i^n(1+\phi_i^n)A(\mathbf{x}_i)+3\epsilon^2\sum_{j\in V(i)}\left(\cot\theta_{ij}+\cot\theta_{ij+}\right)}{2\epsilon^2A(\mathbf{x}_i)}\right)\le 1.$$

Then, the temporal step size Δt must satisfy the following condition:

$$\Delta t \le \frac{2\epsilon^2A(\mathbf{x}_i)}{\phi_i^n(1+\phi_i^n)\,2A(\mathbf{x}_i)+3\epsilon^2\sum_{j\in V(i)}\left(\cot\theta_{ij}+\cot\theta_{ij+}\right)}.$$

Since $0 < \phi_i^n(1 + \phi_i^n) < 2$ holds, we have the following constraint:

$$\Delta t \leq \frac{2\epsilon^2 A(\mathbf{x}_i)}{4A(\mathbf{x}_i) + 3\epsilon^2 \sum\limits_{j\in V(i)} \left(\cot\theta_{ij} + \cot\theta_{ij+}\right)}. \tag{3.7}$$

Therefore, by using a temporary step size Δt that satisfies Eq (3.7), the condition $|\phi_i^{n+1}| \leq 1$ is ensured.

Case 4. $-1 \leq \phi_i^n < 0$

For $-1 \leq \phi_i^n < 0$, we rewrite as $0 < -\phi_i^n \leq 1$. Let us consider multiplying both sides of (3.3) by -1:

$$-\phi_i^{n+1} = -\phi_i^n + \frac{\Delta t}{\epsilon^2}\left[-\phi_i^n - (-\phi_i^n)^3\right] + \frac{3\Delta t}{A(\mathbf{x}_i)} \sum_{j\in V(i)} \frac{\cot\theta_{ij} + \cot\theta_{ij+}}{2}(-\phi_j^n - (-\phi_i^n)).$$

Considering the right side of the above equation for $-\phi_i^n$, we can prove that

$$\begin{aligned}\Delta t &\leq \min_{1\leq i\leq N}\left(\frac{2\epsilon^2 A(\mathbf{x}_i)}{4A(\mathbf{x}_i) + 3\epsilon^2 \sum\limits_{j\in V(i)} \left(\cot\theta_{ij} + \cot\theta_{ij+}\right)}, \frac{2A(\mathbf{x}_i)}{3\sum\limits_{1\leq i\leq N} \left(\cot\theta_{ij} + \cot\theta_{ij+}\right)}\right) \\ &= \frac{2\epsilon^2 A(\mathbf{x}_i)}{4A(\mathbf{x}_i) + 3\epsilon^2 \sum\limits_{j\in V(i)} \left(\cot\theta_{ij} + \cot\theta_{ij+}\right)},\end{aligned}$$

which guarantees $| - \phi_i^{n+1}| = |\phi_i^{n+1}| \leq 1$. Hence, $\|\phi^{n+1}\|_\infty \leq 1$ holds for Δt satisfying the time step constraint as

$$\Delta t \leq \min_{1\leq i\leq N} \frac{2\epsilon^2 A(\mathbf{x}_i)}{4A(\mathbf{x}_i) + 3\epsilon^2 \sum\limits_{j\in V(i)} \left(\cot\theta_{ij} + \cot\theta_{ij+}\right)}.$$

We consider a triangular mesh $\mathcal{T}_h = (V_h, E_h, F_h)$ of a smooth closed surface $\mathcal{S}$ (e.g., a sphere or torus). Here, V_h is the set of vertices, E_h is the set of edges, and F_h is the set of triangular faces. For $e = \overline{pq} \in E_h$, we denote by $|e|$ the length of the edge e measured on the piecewise-linear surface; equivalently, if $\mathcal{S} \subset \mathbb{R}^3$ is embedded, $|e|$ is the Euclidean length of the segment joining the endpoints p and q. The global mesh size is defined by

$$h := \max_{e\in E_h} |e|.$$

We assume that $\{\mathcal{T}_h\}$ is a shape-regular, quasi-uniform family of triangulations. Specifically, there exists $\theta_* > 0$ such that every triangle $T \in F_h$ has all interior angles bounded below by θ_*. Moreover, there exist constants $c_1, c_2 > 0$, independent of h, such that $c_1 h \leq h_T \leq c_2 h$ for every element $T \in F_h$, where $h_T := \max\limits_{e\subset T} |e|$. Let $A(\mathbf{x}_i)$ denote the mixed area associated with a vertex $\mathbf{x}_i \in V_h$, and let

$$W_i := \sum_{j\in V(i)} \left(\cot\theta_{ij} + \cot\theta_{ij+}\right)$$

be the standard cotangent-weight sum at $\mathbf{x}_i$, where θ_{ij} and θ_{ij+} are the angles opposite the edge (i, j) in the two adjacent triangles. Then, by shape-regularity and quasi-uniformity, there exist h-independent positive constants

$$C_A^- := \inf_h \min_i \frac{A(\mathbf{x}_i)}{h^2}, \qquad C_A^+ := \sup_h \max_i \frac{A(\mathbf{x}_i)}{h^2}, \qquad C_w^+ := \sup_h \max_i W_i,$$

such that, for all vertices $\mathbf{x}_i$,

$$C_A^- h^2 \;\le\; A(\mathbf{x}_i) \;\le\; C_A^+ h^2, \qquad W_i \;\le\; C_w^+. \tag{3.8}$$

Let us recall the pointwise stability restriction (3.2):

$$\Delta t \le \min_{1\le i\le N} \frac{2\epsilon^2 A(\mathbf{x}_i)}{4A(\mathbf{x}_i) + 3\epsilon^2 \sum_{j\in V(i)} \left(\cot\theta_{ij} + \cot\theta_{ij+}\right)}.$$

Set $f(A, W) := \dfrac{2\epsilon^2 A}{4A + 3\epsilon^2 W}$. A direct calculation shows $\dfrac{\partial f}{\partial A} > 0$ and $\dfrac{\partial f}{\partial W} < 0$, i.e., f is increasing in A and decreasing in W. Using this monotonicity and (3.8), we bound each fraction from below by

$$\frac{2\epsilon^2 A(\mathbf{x}_i)}{4A(\mathbf{x}_i) + 3\epsilon^2 W_i} \;\ge\; \frac{2\epsilon^2 C_A^- h^2}{4C_A^+ h^2 + 3\epsilon^2 C_w^+}.$$

Taking the minimum over i, we obtain the following global, h-explicit sufficient CFL condition:

$$\Delta t \le \frac{2\epsilon^2 C_A^- h^2}{4C_A^+ h^2 + 3\epsilon^2 C_w^+}. \tag{3.9}$$

Here, the constants $C_A^\pm$ and C_w^+ depend only on the mesh regularity and on the geometry of $\mathcal{S}$, and are independent of the global mesh size h. From (3.9), we conclude that there are two regimes. (i) In the fine-mesh limit $h \to 0$, $\Delta t \le \dfrac{2C_A^-}{3C_w^+} h^2$, i.e., $\Delta t = O(h^2)$. (ii) On coarser meshes, the bound saturates at the h-independent value $\Delta t \le \dfrac{C_A^-}{2C_A^+}\epsilon^2$. For quasi-uniform refinements on the sphere or torus, this recovers the expected $O(h^2)$ scaling of explicit diffusion-type CFL restrictions on surfaces.

We study the surface AC equation on the unit sphere $\mathcal{S}_{R_0}$ with $R_0 = 1$. The surface is discretized by shape-regular, quasi-uniform icosahedral refinements (levels 0 to 7). Spatial operators use the cotangent Laplace–Beltrami operator with lumped mixed areas. We denote the mean geodesic edge length by $h_{\text{geo}} := \dfrac{1}{|E_h|} \sum_{e\in E_h} R_0 \arccos\left(\dfrac{\mathbf{x}_i \cdot \mathbf{x}_j}{R_0^2}\right)$. Time integration is fully explicit. To maintain a fixed number of mesh edges across the diffuse interface, we set $\epsilon = \dfrac{m h_{\text{geo}}}{2\sqrt{2}\tanh^{-1}(0.9)}$, $m = 8$. With this choice, the ± 0.9 transition layer spans approximately m edge lengths at every refinement level. Consequently, the interfacial resolution and the CFL behavior are consistent under mesh refinement. For each refinement level (see Figure 2), we determine the largest stable time step by bisection. A

step is declared stable over a short horizon of 300 iterations if two conditions are met: (i) no blow-up or overshoot, that is, $|\phi| \leq 1 + 10^{-3}$ at all nodes; (ii) monotone decay of the discrete energy $\mathcal{E}_h(\phi) = -\langle \phi, L\phi \rangle_A + \frac{1}{\epsilon^2} \sum_i A_i \frac{1}{4} \left(\phi_i^2 - 1\right)^2$, where $\langle u, v \rangle_A := \sum_i A_i u_i v_i$ is the A-weighted inner product and L is the mass-lumped cotangent stiffness.

Initial conditions are small random perturbations $\phi(x, y, z, 0) = \text{rand(x, y, z)}$ where $\text{rand}(x, y, z)$ represents a random number in $[-0.1, 0.1]$. In Figure 3(a), the log-log plot of $\Delta t_{\max}$ versus h has slope ≈ 2, confirming the quadratic scaling $\Delta t_{max} = O(h^2)$. Correspondingly, in Figure 3(b), $\Delta t_{\max}/h^2$ approaches a flat plateau of about 0.23 on the finest meshes. This trend is consistent with the h-explicit bound in (3.9). Figures 4(a)–(d) show smooth, curvature-driven coarsening without spurious oscillations, indicating that the explicit scheme run with $\Delta t = \Delta t_{\max}$ is stable and faithfully captures the asymptotic phase separation dynamics under noisy initial data.

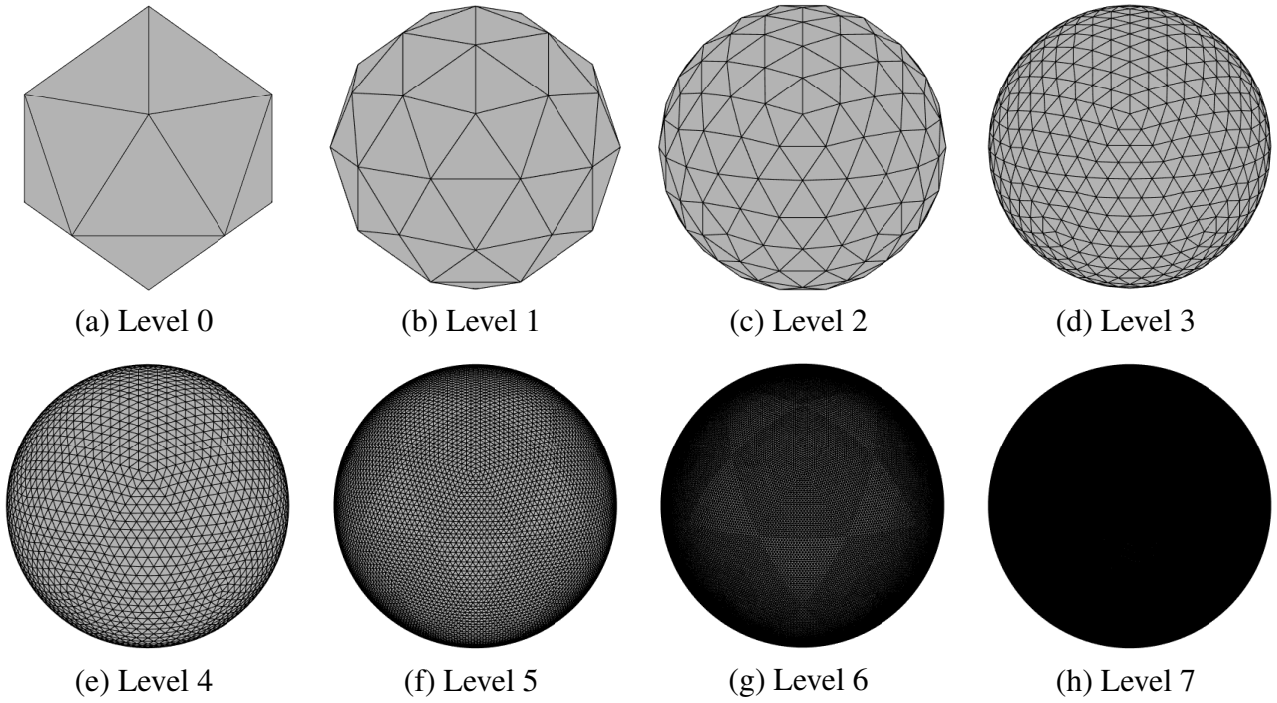

(a) Level 0 (b) Level 1 (c) Level 2 (d) Level 3

(e) Level 4 (f) Level 5 (g) Level 6 (h) Level 7

Figure 2. Triangulations of the sphere obtained by successive icosahedral refinements: (a)–(h) correspond to levels 0 to 7, from coarse to fine.

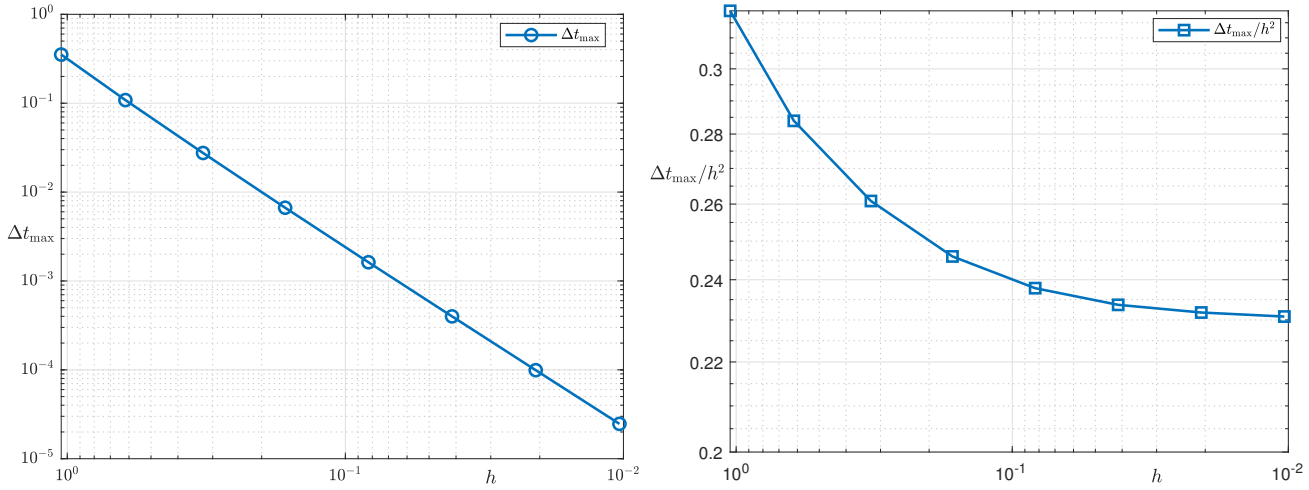

Figure 3. (a) Maximal stable step $\Delta t_{\max}$ versus mesh size h (log-log). A least-squares fit has slope ≈ 2, confirming the quadratic scaling $\Delta t_{\max} = O(h^2)$. (b) $\Delta t_{\max}/h^2$ versus h.

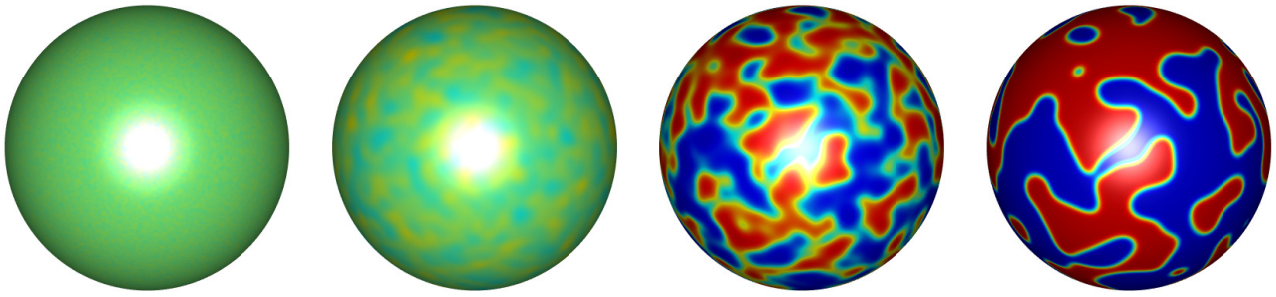

Figure 4. Surface AC evolution on the Level 7 triangulated sphere from a randomly perturbed initial state. Snapshots at (a) $t = 1\Delta t$, (b) $t = 24\Delta t$, (c) $t = 97\Delta t$, and (d) $t = 240\Delta t$.

Remark. In addition to the explicit Euler method, one may also consider higher-order explicit Runge–Kutta (RK) schemes [46–52]. From the stability perspective, the essential CFL-type restriction remains unchanged. Although higher-order RK schemes possess larger stability regions than the explicit Euler method and hence permit a larger admissible constant in the bound, the quadratic dependence on the spatial mesh size h and the interfacial parameter ϵ is preserved. Consequently, explicit RK methods improve temporal accuracy and allow moderately larger time steps in practice, but they do not fundamentally overcome the severe CFL-type limitation. The theoretical bound established in this work therefore provides a rigorous guideline not only for the explicit Euler method but also for general explicit Runge–Kutta integrators.

4. Numerical tests

We will conduct computational tests to demonstrate the sharp estimation of the time step restriction of the fully explicit numerical method. In addition, we will perform several characteristic

computational tests, such as motion by mean curvature on spherical and complex surfaces.

4.1. Optimal estimation of the time step for the maximum principle

We conduct a numerical experiment by presenting a counterexample to verify that the time step constraint for the maximum principle is an accurate estimation. As a simple example, we consider the following seven points that construct a discrete surface: $\mathbf{x}_i = (0, 0, 0.01)$ and $\mathbf{x}_{ik} = (0.1\cos[\pi(k-1)/3], 0.1\sin[\pi(k-1)/3], 0)$ for $k = 1, 2, \ldots, 7$.

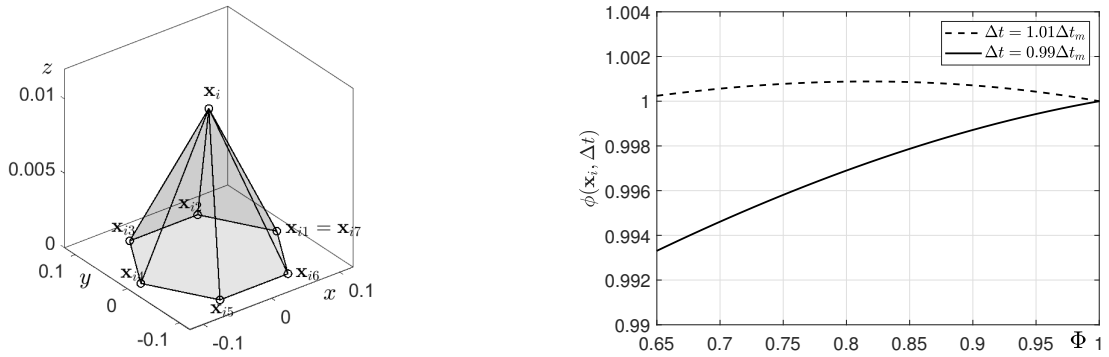

(a) (b)

Figure 5. (a) Given seven points. (b) The value of $\phi(\mathbf{x}_i, \Delta t)$ with respect to the value of Φ.

The given points are shown in Figure 5(a). Then, we set the initial condition as follows:

$$\phi(\mathbf{x}, 0) = \begin{cases} \Phi, & \text{if } \mathbf{x} = \mathbf{x}_i, \\ 1, & \text{otherwise,} \end{cases}$$

where $0 \le \Phi \le 1$. The maximum time step size is given by Theorem 1 as

$$\Delta t_{max} = \min_{1 \le i \le N} \frac{2\epsilon^2 A(\mathbf{x}_i)}{4A(\mathbf{x}_i) + 3\epsilon^2 \sum_{j \in V(i)} \left(\cot\theta_{ij} + \cot\theta_{ij+}\right)}.$$

Here, we use $\epsilon = 0.5$. We consider two time steps $\Delta t = 1.01\Delta t_{max}$ and $\Delta t = 0.99\Delta t_{max}$ for $0 \le \Phi \le 1$. Figure 5(b) shows the values of $\phi(\mathbf{x}_i, \Delta t)$ for $\Delta t = 1.01\Delta t_{max}$ and $\Delta t = 0.99\Delta t_{max}$. From the results in Figure 5(b), we observe that while the maximum principle is preserved true for $\Delta t = 0.99\Delta t_{max}$, counterexamples are shown where the maximum principle is not satisfied for $\Delta t = 1.01\Delta t_{max}$.

4.2. Phase separation with a randomly perturbed initial condition

To validate the robustness of the proposed method, we consider a numerical test case in which the surface AC was solved on a triangulated sphere (Figure 6(a)) with a randomly perturbed initial condition (Figure 6(b)):

$$\phi(x, y, z, 0) = \text{rand}(x, y, z),$$

where rand(x, y, z) represents a random number in $[-1, 1]$. Here, the parameter values are used as $\Delta t = 0.00177$, $h = h_{ave} = 0.17462$, and $\epsilon = \epsilon_m = \dfrac{mh}{2\sqrt{2}\tanh^{-1}(0.9)}$, $m = 3$.

The purpose of this numerical experiment is to assess whether the scheme can handle noisy inputs while still reproducing the expected phase separation behavior. At $t = 0$, the initial condition is highly disordered, but within a short time ($t = 5\Delta t$), local domains emerge. These domains subsequently coarsen and interfaces shrink under curvature-driven dynamics at ($t = 20\Delta t$) and ($t = 50\Delta t$), and eventually the system approaches a homogeneous equilibrium state at $t = 700\Delta t$. The numerical results indicate that the explicit scheme remains stable even under highly noisy initial data, as no spurious oscillations or numerical instabilities are observed throughout the evolution. Moreover, the solution reproduces the theoretically expected asymptotic behavior of the AC equation on surfaces, namely curvature-driven domain coarsening and convergence to a homogeneous equilibrium. This confirms that the proposed scheme is both robust to noise and faithful to the asymptotic dynamics of phase separation.

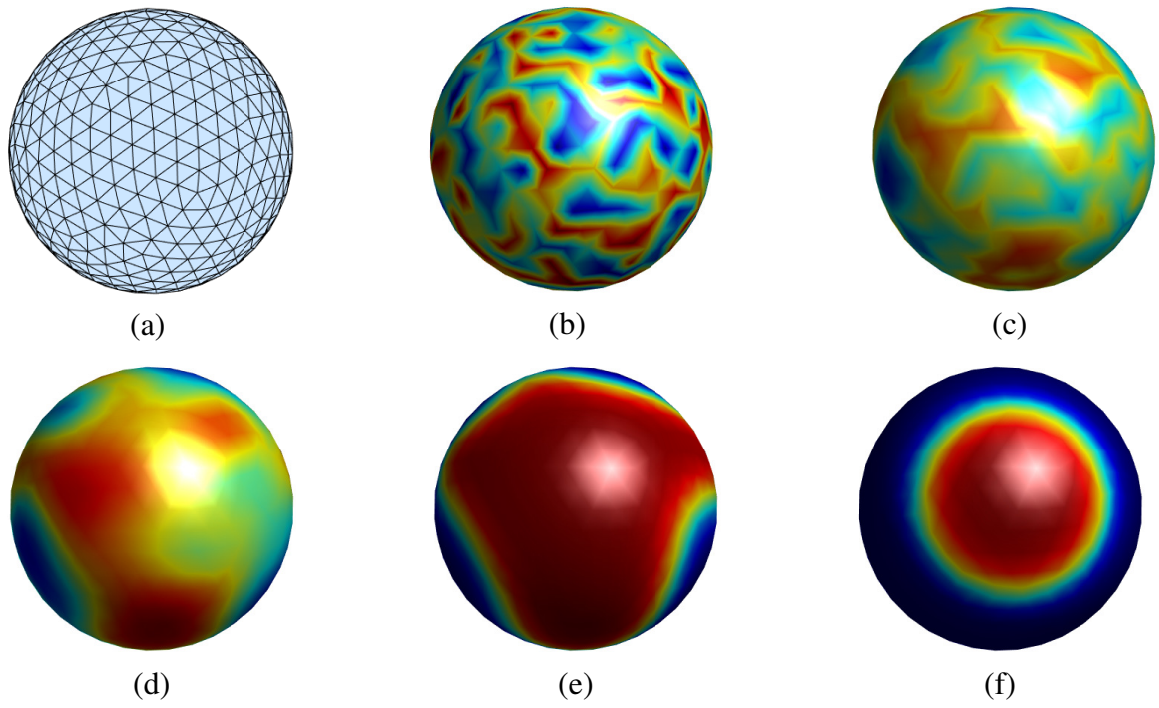

Figure 6. Phase separation dynamics of the surface AC on a triangulated sphere with a randomly perturbed initial condition. The purpose of this test is to assess the robustness of the method against noisy inputs. Shown are (a) the computational triangulated domain, and numerical solutions at (b) $t = 0$, (c) $t = 5\Delta t$, (d) $t = 20\Delta t$, (e) $t = 50\Delta t$, and (f) $t = 700\Delta t$. The numerical solution evolves stably from a highly disordered state, with local domains emerging, interfaces coarsening under curvature-driven motion, and eventual convergence to a homogeneous equilibrium.

4.3. Evolution on a sphere

We examine the movement of a circular interface on a sphere, which evolves according to in-surface curvature motion [53].

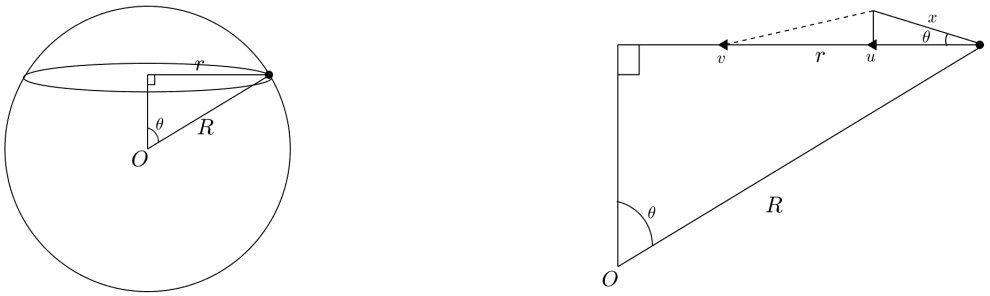

(a) (b)

Figure 7. Schematic to show (a) parameters on the circular interface of the sphere and (b) the zoomed description of the triangular part of (a).

As shown in Figure 7(a), R and r represent the radii of the sphere and circular interface on the sphere, respectively. Let $v = -1/r$ denote the curvature of the circle, let x be the tangential component of v, and let u be the component of x directed toward the center of the circle. Then, from Figure 7(b), we can determine that $u = -\frac{1}{r}\cos^2\theta$, where θ is the angle between x and u. Thus, we have

$$\frac{dr}{dt} = u = -\frac{1}{r}\cos^2\theta = \frac{r^2 - R^2}{rR^2}. \tag{4.1}$$

By solving Eq (4.1), we obtain the analytical solution for $r(t)$:

$$r(t) = \sqrt{R^2 - (R^2 - r_0^2)e^{2t/R^2}}. \tag{4.2}$$

On a triangulated sphere, we validate the property for motion by mean curvature. The initial condition $\phi(x, y, z, 0)$ (see Figure 8) is considered as follows:

$$\phi(x, y, z, 0) = \tanh\left(\frac{R_0\frac{\pi}{3} - R_0\left|\arccos\left(\frac{z}{R_0}\right)\right|}{\sqrt{2}\epsilon}\right),$$

where $R_0 = 7$, $\epsilon = \epsilon_m = \dfrac{mh}{2\sqrt{2}\tanh^{-1}(0.9)}$, $m = 12$, and $h = h_{ave}$. The parameter values are used as $\Delta t = 0.001$, $h_{ave} = 0.17773$. The evolutionary numerical behaviors of the AC equation can be seen in Figures 8(a)–(d). On the triangulated sphere, the initial spherical cap shrinks over time, by motion by mean curvature along the curvature of the sphere. From the numerical results of the long-time simulation using the proposed method, we observed that the motion by mean curvature stably evolves until $t = 30000\Delta t$.

The process of changing the initial radius of the spherical cap over time can be seen in Figure 9, and it can be seen that the analytical and numerical solutions match well.

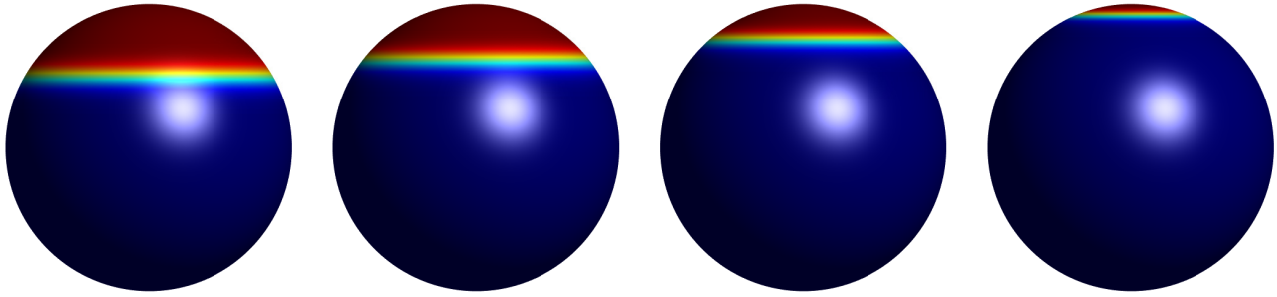

(a) (b) (c) (d)

Figure 8. Motion by mean curvature on the triangulated sphere at (a) $t = 0$, (b) $t = 10000\Delta t$, (c) $t = 20000\Delta t$, and (d) $t = 30000\Delta t$.

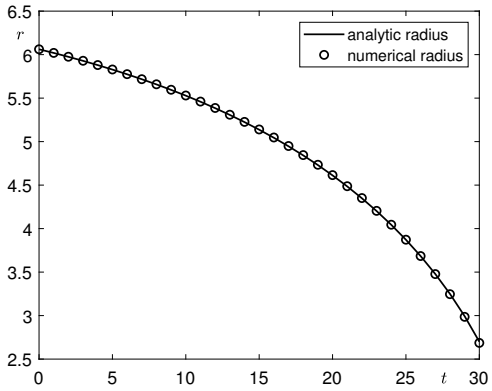

Figure 9. Analytic radii and numerical radii when $m = 12$.

4.4. Evolution on a complex surface

We perform a numerical simulation of motion by mean curvature on a complex surface such as a bunny-shaped surface. The initial condition is set to a triangle shape as shown in Figure 10(a):

$$\phi(x, y, z, 0) = \begin{cases} 1 & \text{if } y > -14\ ,\ y < \sqrt{3}|(x - 10.0)|,\ z > -4.00, \\ -1 & \text{otherwise.} \end{cases}$$

Here, the parameter values are $\Delta t = 0.001$, $h = h_{ave} = 0.72644$, and $\epsilon = \epsilon_m = \dfrac{mh}{2\sqrt{2}\tanh^{-1}(0.9)}$, $m = 4$. On a bunny surface, the evolutionary dynamics of the surface AC equation can be seen in Figures 10(b)–(d). The numerical behavior of the smoothed triangle (Figure 10(b)) is transformed to the rounded triangle (Figure 10(c)). At the final time $t = 30000\Delta t$, the rounded triangle shrinks and transforms into a small circle, which is obtained by the mean curvature flow of the surface AC equation.

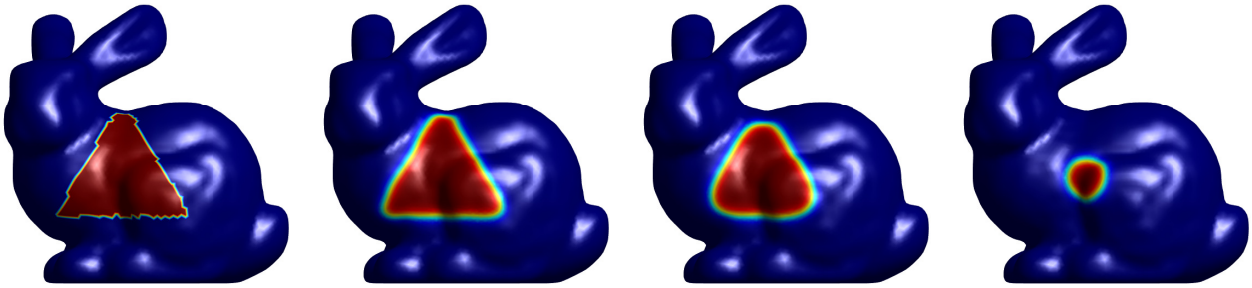

(a) (b) (c) (d)

Figure 10. Motion by mean curvature on the triangulated bunny surface at (a) $t = 0$, (b) $t = 1000\Delta t$, (c) $t = 5000\Delta t$, and (d) $t = 30000\Delta t$.

5. Conclusions

In conclusion, this study presented a comprehensive stability analysis of the fully explicit numerical scheme for the surface AC equation. The implementation of a discrete surface Laplace operator on a triangular mesh yields a simple and efficient discrete equation. Despite this simplicity, there is a moderate time step restriction, and it is necessary to determine the maximum time step for practical applications. Through extensive computational testing, we validated this theoretical maximum time step and confirmed the accuracy and reliability of the theoretical analysis. These findings contribute to the development of more robust numerical schemes for the surface AC equation, with implications for improved computational efficiency and accuracy in practical applications. Although the proposed explicit scheme provides a sharp and rigorous stability condition, its efficiency remains limited by the time step restriction. Future research could investigate one-step adaptive time-stepping or stabilized semi-implicit approaches to reduce this constraint. In addition, a promising direction is to generalize the analysis and algorithmic ideas to the nonlocal ternary viscous CH model [54] on evolving curved surfaces. Finite-range nonlocal interactions are essential for capturing sharp interfaces and for computing contact angles among three phases with high accuracy. Building on the current stability method, it is possible to design high-order explicit hybrid algorithms that combine time-splitting with the spectral deferred correction method. A practical starting point is a second-order Fourier spectral scheme coupled with a strong-stability-preserving RK integrator, which avoids nonlinear iterations and achieves spectral accuracy in space, followed by a semi-implicit spectral deferred correction upgrade to raise the temporal order. Companion numerical studies should compare dynamical behavior with local ternary CH, constrained ternary AC, and modified CH variants, and should include stability assessments and contact-angle benchmarks. The viscoelastic creep behavior observed in nonlocal simulations may inform the design of high-strength yet compliant fiber-composite materials. Extensions to convection-coupled nonlocal ternary viscous CH systems on surfaces would further expand the range of applications. These directions would further broaden the applicability of the method in scientific and engineering contexts.

Use of AI tools declaration

The authors declare they have not used Artificial Intelligence (AI) tools in the creation of this article.

Acknowledgment

The first author (Hyundong Kim) was supported by the Basic Science Research Program through the National Research Foundation of Korea (NRF) funded by the Ministry of Education, Republic of Korea (NRF-2021R1A6A1A0304432, RS-2025-25415913). Jian Wang was supported by The Natural Science Foundation of Jiangsu Province (Grants No BK20240689). Junseok Kim was supported by the National Research Foundation (NRF), Korea, under project BK21 FOUR. The authors would like to thank the reviewers for their valuable comments and constructive suggestions, which helped improve the quality of this paper.

Conflicts of interest

The authors declare there is no conflict of interest.

References

1. S. M. Allen, J. W. Cahn, A microscopic theory for antiphase boundary motion and its application to antiphase domain coarsening, *Acta Metall.*, **27** (1979), 1085–1095. https://doi.org/10.1016/0001-6160(79)90196-2
2. Y. Choi, Y. Li, C. Lee, H. Kim, J. Kim, Explicit hybrid numerical method for the Allen–Cahn type equations on curved surfaces, *Numer. Math. Theory Methods Appl.*, **14** (2021), 797–810. https://doi.org/10.4208/nmtma.OA-2020-0155
3. Y. Li, S. Guo, Triply periodic minimal surface using a modified Allen–Cahn equation, *Appl. Math. Comput.*, **295** (2017), 84–94. https://doi.org/10.1016/j.amc.2016.10.005
4. L. Ortellado, L. R. Gómez, Phase field modeling of dendritic growth on spherical surfaces, *Front. Mater.*, **7** (2020), 163. https://doi.org/10.3389/fmats.2020.00163
5. R. Parthasarathy, C. H. Yu, J. T. Groves, Curvature-modulated phase separation in lipid bilayer membranes, *Langmuir*, **22** (2006), 5095–5099. https://doi.org/10.1021/la060390o
6. F. A. Heberle, G. W. Feigenson, Phase separation in lipid membranes, *Cold Spring Harbor Perspect. Biol.*, **3** (2011), a004630. https://doi.org/10.1101/cshperspect.a004630
7. K. Yokota, T. Ogino, Phase separation in lipid bilayer membranes induced by intermixing at a boundary of two phases with different components, *Chem. Phys. Lipids*, **191** (2015), 147–152. https://doi.org/10.1016/j.chemphyslip.2015.09.001
8. S. Lai, B. Jiang, Q. Xia, B. Xia, J. Kim, Y. Li, On the phase-field algorithm for distinguishing connected regions in digital model, *Eng. Anal. Boundary Elem.*, **168** (2024), 105918. https://doi.org/10.1016/j.enganabound.2024.105918
9. B. Fu, D. Cai, X. Kong, R. Gao, J. Yang, On the numerical approximation of a phase-field volume reconstruction model: Linear and energy-stable leap-frog finite difference scheme, *Commun. Nonlinear Sci. Numer. Simul.*, **151** (2025), 109104. https://doi.org/10.1016/j.cnsns.2025.109104
10. Y. Li, S. Lan, X. Liu, B. Lu, L. Wang, An efficient volume repairing method by using a modified Allen–Cahn equation, *Pattern Recognit.*, **107** (2020), 107478. https://doi.org/10.1016/j.patcog.2020.107478

11. Y. Jin, S. Kwak, S. Ham, J. Kim, A fast and efficient numerical algorithm for image segmentation and denoising, *AIMS Math.*, **9** (2024), 5015–5027. https://doi.org/10.3934/math.2024243
12. S. Su, J. Yang, Unconditionally stable algorithm with unique solvability for image inpainting using a penalized Allen–Cahn equation, *Commun. Nonlinear Sci. Numer. Simul.*, **142** (2025), 108503. https://doi.org/10.1016/j.cnsns.2024.108503
13. H. Kim, S. Kang, G. Lee, S. Yoon, J. Kim, Shape transformation on curved surfaces using a phase-field model, *Commun. Nonlinear Sci. Numer. Simul.*, **133** (2024), 107956. https://doi.org/10.1016/j.cnsns.2024.107956
14. A. Jiang, Y. Wang, F. Zheng, X. Xiao, A convective Allen–Cahn model for the two-and three-dimensional shape transformations of non-contact objects, *Comput. Math. Appl.*, **188** (2025), 72–82. https://doi.org/10.1016/j.camwa.2025.03.018
15. S. Ham, H. Kim, Y. Hwang, S. Kwak, Jyoti, J. Wang, et al., A novel phase-field model for three-dimensional shape transformation, *Comput. Math. Appl.*, **176** (2024), 67–76. https://doi.org/10.1016/j.camwa.2024.09.006
16. Z. Han, H. Xu, J. Wang, A simple shape transformation method based on phase-field model, *Comput. Math. Appl.*, **147** (2023), 121–129. https://doi.org/10.1016/j.camwa.2023.07.020
17. J. He, Solving a class of shape-transforming phase-field models using the lattice Boltzmann method, *Eng. Anal. Boundary Elem.*, **179** (2025), 106358. https://doi.org/10.1016/j.enganabound.2025.106358
18. Y. Wang, X. Xiao, X. Feng, An efficient maximum bound principle preserving p-adaptive operator-splitting method for three-dimensional phase field shape transformation model, *Comput. Math. Appl.*, **120** (2022), 78–91. https://doi.org/10.1016/j.camwa.2022.06.015
19. H. Zhao, B. D. Storey, R. D. Braatz, M. Z. Bazant, Learning the physics of pattern formation from images, *Phys. Rev. Lett.*, **124** (2020), 060201. https://doi.org/10.1103/PhysRevLett.124.060201
20. X. Hu, Q. Xia, B. Xia, Y. Li, A second-order accurate numerical method with unconditional energy stability for the Lifshitz–Petrich equation on curved surfaces, *Appl. Math. Lett.*, **163** (2025), 109439. https://doi.org/10.1016/j.aml.2024.109439
21. B. Xia, X. Xi, R. Yu, P. Zhang, Unconditional energy-stable method for the Swift–Hohenberg equation over arbitrarily curved surfaces with second-order accuracy, *Appl. Numer. Math.*, **198** (2024), 192–201. https://doi.org/10.1016/j.apnum.2024.01.005
22. Y. Li, R. Liu, Q. Xia, C. He, Z. Li, First- and second-order unconditionally stable direct discretization methods for multi-component Cahn–Hilliard system on surfaces, *J. Comput. Appl. Math.*, **401** (2022), 113778. https://doi.org/10.1016/j.cam.2021.113778
23. Q. Pan, C. Chen, Y. J. Zhang, X. Yang, A novel hybrid IGA-EIEQ numerical method for the Allen–Cahn/Cahn–Hilliard equations on complex curved surfaces, *Comput. Methods Appl. Mech. Eng.*, **404** (2023), 115767. https://doi.org/10.1016/j.cma.2022.115767
24. Q. Pan, J. Zhang, T. Rabczuk, C. Chen, X. Yang, Numerical algorithms of subdivision-based IGA-EIEQ method for the molecular beam epitaxial growth models on complex surfaces, *Comput. Mech.*, **72** (2023), 927–948. https://doi.org/10.1007/s00466-023-02319-6

25. Q. Pan, T. Rabczuk, G. Xu, C. Chen, Isogeometric analysis for surface PDEs with extended Loop subdivision, *J. Comput. Phys.*, **398** (2019), 108892. https://doi.org/10.1016/j.jcp.2019.108892

26. Q. Pan, T. Rabczuk, C. Chen, Subdivision based isogeometric analysis for geometric flows, *Int. J. Numer. Methods Eng.*, **123** (2022), 610–633. https://doi.org/10.1002/nme.6870

27. J. Shen, T. Tang, J. Yang, On the maximum principle preserving schemes for the generalized Allen–Cahn equation, *Commun. Math. Sci.*, **14** (2016), 1517–1534. https://doi.org/10.4310/CMS.2016.v14.n6.a3

28. X. Feng, A. Prohl, Numerical analysis of the Allen–Cahn equation and approximation for mean curvature flows, *Numer. Math.*, **94** (2003), 33–65. https://doi.org/10.1007/s00211-002-0413-1

29. H. Kim, G. Lee, S. Kang, S. Ham, Y. Hwang, J. Kim, Hybrid numerical method for the Allen–Cahn equation on nonuniform grids, *Comput. Math. Appl.*, **158** (2024), 167–178. https://doi.org/10.1016/j.camwa.2024.01.016

30. Y. Hwang, Jyoti, S. Kwak, H. Kim, J. Kim, An explicit numerical method for the conservative Allen–Cahn equation on a cubic surface, *AIMS Math.*, **9** (2024), 34447–34465. https://doi.org/10.3934/math.20241641

31. Y. Hwang, S. Ham, H. G. Lee, H. Kim, J. Kim, Numerical algorithms for the phase-field models using discrete cosine transform, *Mech. Res. Commun.*, **139** (2024), 104305. https://doi.org/10.1016/j.mechrescom.2024.104305

32. H. Zamani-Gharaghoshi, M. Dehghan, M. Abbaszadeh, Numerical solution of Allen–Cahn model on surfaces via an effective method based on generalized moving least squares (GMLS) approximation and the closest point approach, *Eng. Anal. Boundary Elem.*, **152** (2023), 575–581. https://doi.org/10.1016/j.enganabound.2023.04.019

33. J. Yang, S. Kang, S. Kwak, J. Kim, The Allen–Cahn equation with a space-dependent mobility and a source term for general motion by mean curvature, *J. Comput. Sci.*, **77** (2024), 102252. https://doi.org/10.1016/j.jocs.2024.102252

34. J. Yang, D. Lee, S. Kwak, S. Ham, J. Kim, The Allen–Cahn model with a time-dependent parameter for motion by mean curvature up to the singularity, *Chaos, Solitons Fractals*, **182** (2024), 114803. https://doi.org/10.1016/j.chaos.2024.114803

35. A.I. Bobenko, B. A. Springborn, A discrete Laplace–Beltrami operator for simplicial surfaces, *Discrete Comput. Geom.*, **38** (2007), 740–756. https://doi.org/10.1007/s00454-007-9006-1

36. H. Kim, *Explicit Time-stepping Approach for Pattern Formation on Evolving Curved Surfaces*, Ph.D thesis, Korea University, 2022.

37. X. Xiao, X. Feng, J. Yuan, The stabilized semi-implicit finite element method for the surface Allen–Cahn equation, *Discrete Contin. Dyn. Syst. - Ser. B*, **22** (2017), 2857–2877. https://doi.org/10.3934/dcdsb.2017154

38. X. Xiao, R. He, X. Feng, Unconditionally maximum principle preserving finite element schemes for the surface Allen–Cahn type equations, *Numer. Methods Partial Differ. Equations*, **36** (2020), 418–438. https://doi.org/10.1002/num.22435

39. V. Mohammadi, D. Mirzaei, M. Dehghan, Numerical simulation and error estimation of the time-dependent Allen–Cahn equation on surfaces with radial basis functions, *J. Sci. Comput.*, **79** (2019), 493–516. https://doi.org/10.1007/s10915-018-0859-7
40. F. Zhang, Y. Xu, F. Chen, R. Guo, Interior penalty discontinuous Galerkin based isogeometric analysis for Allen–Cahn equations on surfaces, *Commun. Comput. Phys.*, **18** (2015), 1380–1416. https://doi.org/10.4208/cicp.010914.180315a
41. R. Courant, K. Friedrichs, H. Lewy, Über die partiellen Differenzengleichungen der mathematischen Physik, *Math. Ann.*, **100** (1928), 32–74. https://doi.org/10.1007/BF01448839
42. M. Desbrun, M. Meyer, P. Schröder, A. H. Barr, Implicit fairing of irregular meshes using diffusion and curvature flow, in *Proceedings of the 26th Annual Conference on Computer Graphics and Interactive Techniques*, (1999), 317–324. https://doi.org/10.1145/311535.311576
43. G. Xu, Convergence of discrete Laplace–Beltrami operators over surfaces, *Comput. Math. Appl.*, **48** (2004), 347–360. https://doi.org/10.1016/j.camwa.2004.05.001
44. G. Xu, Convergent discrete Laplace–Beltrami operators over triangular surfaces, *Geom. Model. Process.*, (2004), 195–204. https://doi.org/10.1109/GMAP.2004.1290041
45. Q. Xia, Q. Yu, Y. Li, A second-order accurate, unconditionally energy stable numerical scheme for binary fluid flows on arbitrarily curved surfaces, *Comput. Methods Appl. Mech. Eng.*, **384** (2021), 113987. https://doi.org/10.1016/j.cma.2021.113987
46. H. Zhang, J. Yan, X. Qian, X. Gu, S. Song, On the preserving of the maximum principle and energy stability of high-order implicit-explicit Runge–Kutta schemes for the space-fractional Allen–Cahn equation, *Numerical Algorithms*, **88** (2021), 1309–1336. https://doi.org/10.1007/s11075-021-01077-x
47. Z. Fu, T. Tang, J. Yang, Energy plus maximum bound preserving Runge–Kutta methods for the Allen–Cahn equation, *J. Sci. Comput.*, **92** (2022), 97. https://doi.org/10.1007/s10915-022-01940-6
48. H. G. Lee, J. Shin, J. Y. Lee, Energy quadratization Runge–Kutta scheme for the conservative Allen–Cahn equation with a nonlocal Lagrange multiplier, *Appl. Math. Lett.*, **132** (2022), 108161. https://doi.org/10.1016/j.aml.2022.108161
49. H. Zhang, L. Liu, X. Qian, S. Song, Quantifying and eliminating the time delay in stabilization exponential time differencing Runge–Kutta schemes for the Allen–Cahn equation, *ESAIM. Math. Model. Numer. Anal.*, **58** (2024), 191–221. https://doi.org/10.1051/m2an/2023101
50. H. Zhang, X. Qian, S. Song, Third-order accurate, large time-stepping and maximum-principle-preserving schemes for the Allen–Cahn equation, *Numerical Algorithms*, **95** (2024), 1213–1250. https://doi.org/10.1007/s11075-023-01606-w
51. Y. Sun, Q. Zhou, Maximum bound principle for matrix-valued Allen–Cahn equation and integrating factor Runge–Kutta method, *Numerical Algorithms*, **97** (2024), 391–429. https://doi.org/10.1007/s11075-023-01708-5
52. D. C. Antonopoulou, G. Karali, D. Li, Optimal error estimates of energy-stable Runge–Kutta methods for the ε-dependent Cahn–Hilliard/Allen–Cahn Equation, *J. Sci. Comput.*, **103** (2025), 68. https://doi.org/10.1007/s10915-025-02895-0

53. S. J. Ruuth, B. Merriman, A simple embedding method for solving partial differential equations on surfaces, *J. Comput. Phys.*, **227** (2008), 1943–1961. https://doi.org/10.1016/j.jcp.2007.10.009

54. Z. Weng, S. Zhai, X. Feng, Numerical approximation of the nonlocal ternary viscous Cahn–Hilliard model based on a high order explicit hybrid algorithm, *SIAM J. Sci. Comput.*, **47** (2025), A2221–A2247. https://doi.org/10.1137/24M1645474

AIMS Press